A comparative analysis of total internal reflection based quasi phase matched broadband second harmonic generation in various configurations of double tapered isotropic semiconductor slab

MINAKSHI DEB BARMA, SUMITA DEB*, ARDHENDU SAHA
Department of Electrical Engineering, National Institute of Technology, Agartala, Barjala, Jirania, Tripura (west), Pin-799046, Tripura, India

A comparative study in terms of peak efficiency and 3 dB bandwidth is made on four different double tapered configurations of isotropic semiconductor material using total internal reflection quasi phase matching based second harmonic generation with due consideration to the optical losses (surface roughness, Goos–Hänchen shift and absorption loss). When the destructive interference effect due to the nonlinear law of reflection has been incorporated, heavy drop has been observed in the peak efficiency with GaAs and ZnSe as the slab material, which can be compensated by the introduction of fractional scenario on replacing the material by ZnTe. Finally the temperature tuning of the centre wavelength corresponding to peak second harmonic conversion efficiency has also been suggested.

(Received September 23, 2015; accepted September 29, 2016)

Keywords: Double tapered configuration, Total internal reflection quasi phase matching, Broadband, Second harmonic generation, Isotropic semiconductor, Nonlinear law of reflection, Temperature tuning

1. Introduction

Quasi-phase-matching (QPM) is a technique commonly used for enhancing the efficiency of nonlinear frequency conversions, such as second harmonic generation (SHG), in cases where perfect phase-matching cannot be achieved. The concept of QPM using total internal reflection (TIR) in a plane parallel slab was first suggested by Armstrong *et. al.* [1] in the year 1962, which has subsequently been demonstrated in isotropic semiconductors (GaAs, ZnSe, ZnS) by a number of eminent researchers for both resonant as well as non-resonant situations [2-4]. Broadband SHG based on this TIR-QPM technique has also been analytically demonstrated in a tapered GaAs as well as ZnSe slab [5] where the interaction length between consecutive reflection bounce points goes on increasing as contrary to a parallel slab having equal bounce lengths. This tapered structure resulted in a broader SH efficiency vs. wavelength spectrum where the reported values correspond to nearly 1 % peak efficiency with 3 dB bandwidth (BW) ranging between 180-200 nm [5]. This peak efficiency can be further elevated by using ZnTe made tapered slab, since optical dispersion in ZnTe is much lower as compared to GaAs and ZnSe [6]. The coherence length for ZnTe is approximately 6 times that of GaAs and ZnSe for the range of fundamental wavelength under consideration. This ensures fractional TIR QPM scenario wherein majority of the bounce lengths acquire a fractional relationship with the coherence length corresponding to the centre wavelength of the input fundamental radiations. Afterwards the 3 dB BW has been significantly broadened by the introduction of a double tapered configuration where a combination of increasing and then decreasing bounce lengths has been achieved [7]. For a double tapered GaAs slab the reported value of 3 dB BW is 573.6 nm with a conversion efficiency of 1.929 % [7]. However, the Rayleigh range of the beam which determines the depth of focus was not considered in any one of these papers related to TIR QPM based broadband SHG [5-7]. The Rayleigh range of the fundamental beam, in fact limits the maximum slab length as used for the three wave interaction phenomena. In the present work, with due consideration for Rayleigh range, the same concept of broadband SHG using TIR QPM technique has been demonstrated analytically in three new double tapered configurations and the results obtained there from has been compared with the original double tapered structure [7]. The effect of nonlinear reflection resulting in a complex destructive interference effect among the collinear and homogeneous SHs, as suggested by Raybaut et al. [8], has also been incorporated in the analysis. Finally the possibility of fine tuning of centre wavelength of the SH spectra by varying the temperature in case of GaAs and ZnSe materials has also been explored.

2. Proposed scheme

We have considered three different double tapered configurations as shown in Fig. 1. The first configuration (Fig. 1(a)) is a wedge shaped double tapered semiconductor slab with a gradually diverging profile, the upper surface is tapered at an angle θ_1 whereas the lower surface is tapered at an angle θ_2, which can be determined by the vertical heights t_1, t_2, t_3, the slab length L and the slanted angle ψ. Fig. 1(b) shows the second configuration where the upper and lower surfaces are inclined at an angle θ_1 and θ_2 respectively with the horizontal base, which can also be expressed in terms of the slab dimensions as in case of first configuration. In the third configuration as shown in Fig. 1(c), the lower surface is parallel to the horizontal base whereas the upper surface is made of two tapered sections connected end to end. The first and second tapered sections can be called as the reverse tapered and forward tapered respectively. Both the reverse and forward tapering angles, i.e., θ_1 and θ_2 respectively, are determined by the slab length L and the vertical heights t_1 and t_2 where $t_1 > t_2$. The forward section length L_F is expressed in terms of the reverse section length L_R as $L_F = \gamma \times L_R$, where γ can be either a positive integer or a positive fraction. From now onwards we will be referring to these three proposed configurations as config.1, config.2 & config.3 respectively (Fig. 1(a-c)).

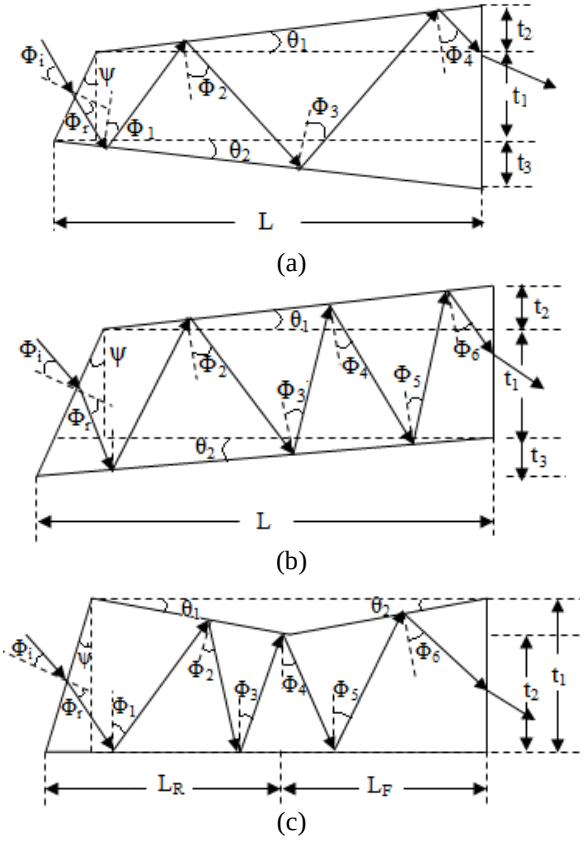

Fig. 1. Schematic representation of optical beam propagation in (a) config. 1, (b) config.2 and (c) config. 3.

When the broadband fundamental laser radiation is made incident on the slanted face of each of the double tapered slabs, at an angle Φ_i, SH will be generated following the same concept as already explained in detail in earlier works [5-7]. The angle of incidence and the length between successive bounces will go on either increasing or decreasing or a combination of both depending on the type of configuration under analysis as the input broadband radiation propagates inside the slab.

Now, for the three proposed double tapered configurations (Fig. 1), the generalized equations for length between consecutive bounces as well as angle of incidence inside the slab can be expressed as shown in the following sections.

2.1. Config. 1

Fig. 2 shows geometrical representation of the bounce length inside the slab. For this proposed slab configuration, the angle of incidence and the length between successive bounces will go on increasing with the propagation of the input broadband radiations throughout the length of the slab.

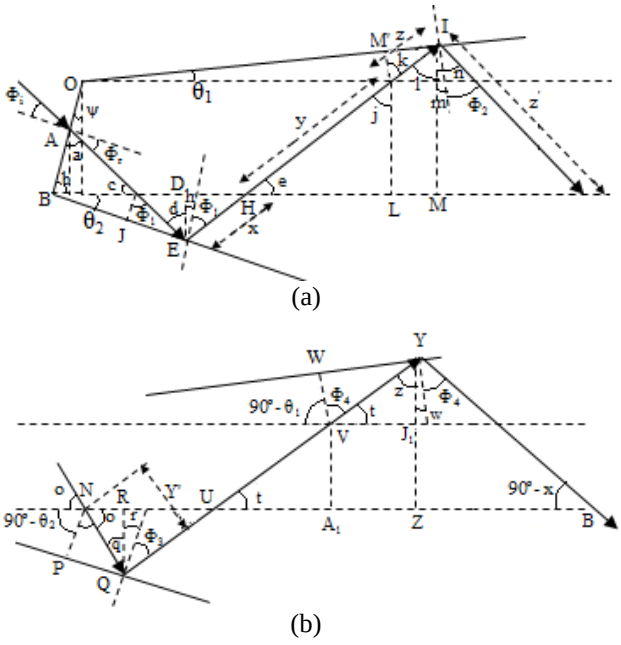

Fig. 2.Geometrical representation of various symbols as used in deriving the generalized expressions of bounce length and incidence angle inside config. 1(a).

Now, the equations for consecutive bounces and angle of incidence inside the slab can be expressed as follows:

L_1 = First interaction length between the entrance point and the first total internal reflection bounce inside the slab

$$= AE = \frac{X\cos\psi}{\sin(\Phi_r+\psi)} + \frac{X\sin\psi\cdot\sin\theta_2}{\cos\Phi_1} + \frac{X\cos\psi\cdot\sin\theta_2}{\cos\Phi_1\tan(\Phi_r+\psi)} \quad (1)$$

Generalization of all even bounce lengths:

$$L_{2n}= \frac{D\, tan\theta_2}{cos\,[\Phi_1+(n-2)\theta_1+(n-1)\theta_2]}+ \frac{t_1}{cos\,(\Phi_1+(n-2)\theta_1+(n-1)\theta_2)}+\frac{D_1 sin\theta_1}{cos\,[\Phi_1+(n-1)(\theta_1+\theta_2)]} \quad (2)$$

Generalization of all odd bounce lengths:

$$L_{2n+1}= \frac{D\sin\theta_2}{\cos[\,(\Phi_1+(n-1)\theta_1+(n-2)\theta_2]}+ \frac{z_{n-1}\cos\,(\Phi_1+(n-3)\theta_1+(n-2)\theta_2+t_1}{\cos\,(\Phi_1+(n-1)\theta_1+(n-2)\theta_2)} \quad (3)$$

Generalization of angle of incident inside the slab:

$$\Phi_n= \Phi_1+(n-1)\,(\theta_1+\theta_2) \quad (4)$$

Where n= number of bounces inside the slab = 1, 2, 3……, x= slant distance of the entrance point from the base of the slab, $\theta_1= \tan^{-1}\frac{t_2}{L-t_1\tan(\psi)}$ and $\theta_2=\tan^{-1}\frac{t_3}{L}$, $\Phi_r = \sin^{-1}\left[\frac{\sin\Phi_i}{n_k}\right]$, n_k is the refractive index corresponding to each individual frequency of the input broadband laser radiation, D represents BD for n=1, BM for n=2 and so on, D_1 representsOK for n=1, OV for n=2 and so on and Φ_1 = First angle of incident inside the slab $= 90^{\circ} + \theta_2 - \Phi_r - \psi$.

2.2. Config. 2

In this case, the angle of incidence and the length between successive bounces will go on decreasing with the propagation of the input broadband radiations inside slab when $\theta_2 > \theta_1$. The length between successive bounces and the angle of incidence inside the slab can be expressed by replacing θ_2 by $(-\theta_2)$ in the expressions derived for config.1.

2.3. Config. 3

Here the angle of incidence and the length between successive bounces will go on decreasing with the progression of the input broadband radiations up to the reverse tapered section length, L_R, after which both the angle of incidence and the bounce length will go on increasing in the forward tapered section length, L_F, till the beam emerges out of the slab.

L_1= length between the entrance point and the first TIR bounce inside the slab = $\frac{x\cos\psi}{\sin(\phi_r+\psi)}$ (5)

The angle of incidence and length between successive bounces inside the slab can be expressed by replacing $\theta_1$and $\theta_2$by $(-\theta_1)$ and $(-\theta_2)$ respectively in the expressions as derived in Ref. [7].

We have analyzed the above mentioned three configurations using GaAs, ZnSe and ZnTe semiconductor materials. In Ref. [5], it has been analytically demonstrated that the use of a tapered semiconductor (GaAs and ZnSe) slab results in flatter spectra of the generated second harmonic BW in comparison to a parallel slab, although the conversion efficiency will be lower in case of the tapered slab. The same explanation holds good for the present configurations as well. Moreover the use of ZnTe as the slab material results in fractional QPM thereby highly enhancing the SH conversion efficiency. The optical phenomena involved will then combine fractional (the interaction lengths (L) between successive bounces are less than the coherence length (L_c)), non resonant (L ≠ odd multiples of L_c) as well as resonant (L = odd multiples of L_c) QPM techniques. Listed below are some basic optical properties of the materials (Table 1), viz. GaAs, ZnSe and ZnTe which are being used in the present analysis.

Table 1. Optical properties of the materials understudy

Semiconductor Material	**Crystal Class**	**d coefficient (pm/V)**	**Absorption coefficient (cm^{-1})**	**p-vValue (nm)**	**Transparency range (μm)**
GaAs	$\bar{4}3\,m$	107 [9, 10]	0.02 [13]	4 [16]	1-15 [9]
ZnSe	$\bar{4}3\,m$	25 [11]	5×10^{-4} [14]	150 [17]	0.5-14 [11]
ZnTe	$\bar{4}3\,m$	90 [12]	0.008 [15]	30 [18]	0.6-25 [15]

The following Sellmeier formulae have been considered for calculating the refractive index of the corresponding materials:

$$\text{GaAs: } n^2(\lambda) = g_o + \frac{g_1}{\lambda_1^{-2}-\lambda^{-2}} + \frac{g_2}{\lambda_2^{-2}-\lambda^{-2}} + \frac{g_3}{\lambda_3^{-2}-\lambda^{-2}} \quad (6)$$

where, n is the temperature dependent refractive index, $\lambda_1 = 0.44313071 + 0.000050564\Delta T$, $\lambda_2 = 0.87464531 + 0.000\ 1913\ \Delta T - 4.882 \times 10^{-7} \times \Delta T^2$, $\lambda_3 = 36.9166 - 0.011622\Delta T$, $g_0 = 5.372514$, $g_1 = 27.83972$, $g_2 = 0.031764 + 4.350 \times 10^{-5}\Delta T + 4.664 \times 10^{-7} \times \Delta T^2$, $g_3 = 0.00143636$.

Equation (6) holds good for wavelength range from 0.97 to 17 μm which covers nearly the entire transmission range of the material [9]. It is also best suited for the calculation of refractive index of the said material measured between room temperature ($\approx 25°C$) and 95° C (=368 K) [9].

$$\text{ZnSe: } n_k^2(\lambda_i, t) = E(t) + \frac{A(t)}{\lambda_i^2-\lambda_u^2} + \frac{B(t)}{\lambda_i^2/\lambda_1^2-1} \quad (7)$$

where, n_k is the wavelength and temperature dependent refractive index, λ_i= wavelength in μm, i= ω for fundamental and 2ω for SH, t = T−293 in Kelvin, T = operating temperature in Kelvin, λ_u = 0.29934 +1.004 $\times 10^{-4}$t in μm, λ_1= 48.38 + 6.29 $\times 10^{-3}$t in μm, E(t)= $9.01536 + 1.4419 \times 10^{-3}t + 3.32973 \times 10^{-7}t^2 - 1.08159 \times 10^{-9}t^3 - 3.88394 \times 10^{-12}t^4$,
A(t) = $0.24482 + 2.77806 \times 10^{-5}t + 1.01703 \times 10^{-8}t^2 - 4.51746 \times 10^{-11}t^3 + 4.18509 \times 10^{-13}t^4$,
B(t) = $3.08889 + 1.13495 \times 10^{-3}t + 2.89063 \times 10^{-7}t^2 - 9.55657 \times 10^{-10}t^3 - 4.76123 \times 10^{-12}t^4$.

Equation (7) covers the wavelength and temperature ranges of 0.55 to 18 μm and 93- 618 K respectively [19].

$$\text{ZnTe: } n^2(\lambda) = 9.92 + \frac{0.42530}{\lambda^2-0.37766^2} + \frac{2.63580}{\lambda^2/_{56.5^2-1}} \quad (8)$$

Equation (8) is best suited for wavelength range of 0.55- 30 μm and temperature at 293 K [19].

In all the proposed configurations, due to non parallel slab profile, the angle of incidence and also the bounce length will undergo a change at each TIR bounce point.

Fig. 3 & 4 below show the variation of the bounce lengths as well as angle of incidence with respect to the number of bounces inside the proposed three slab configurations respectively. Since the angle of incidence changes at each TIR bounce point, the effective d-coefficient also undergoes change in its value at each reflection bounce.

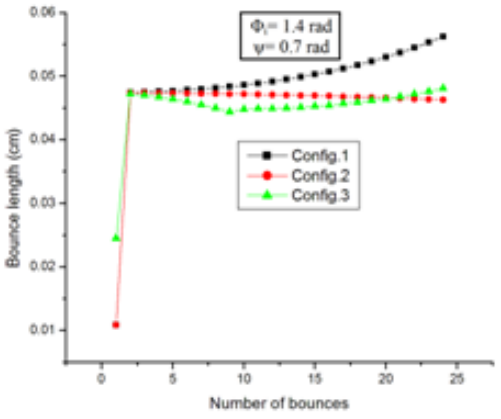

Fig. 3. Variation of bounce length w.r.t. number of bounces

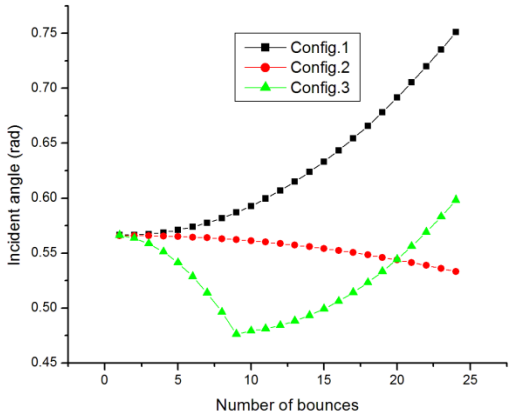

Fig. 4. Variation of angle of incidence w.r.t. number of bounces

3. Effect of nonlinear law of reflection

When a fundamental optical beam is reflected into a nonlinear medium, a collinear SH is generated following the usual phenomena of three wave interaction. However, in order to satisfy the conservation of momentum, a homogeneous SH field is generated according to the following generalized Snell-Descartes law [20]:

$$n_\omega sin\phi_\omega = n_{2\omega} sin\phi_{2\omega} \quad (9)$$

Due to optical dispersion, the incidence angle of the fundamental wave (ϕ_ω) and that of the generated SH wave($\phi_{2\omega}$) are not equal and the small variation in incidence angle as shown in Fig. 5 can be expressed as:

$$\delta\phi \approx -\left(\delta n/_n\right) tan\phi_\omega \quad (10)$$

where, $n_\omega \approx n_{2\omega} = n$ and $\delta n = n_{2\omega} - n_\omega$ is the optical dispersion [8].

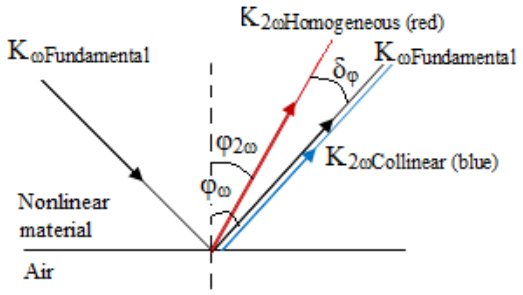

Fig. 5. Generation of collinear SH due to conventional 3-wave mixing and homogeneous SH at an angular shift δφ according to nonlinear law of reflection

Raybaut *et. al.* [8] demonstrated that when a fundamental wave propagates through the parallel semiconductor slab, at each TIR bounce point, two SHs will be generated. First generated wave is the collinear SH due to nonlinear interaction of the fundamental beam according to Fresnel three waves mixing. Second generated wave is the homogeneous SH radiated to satisfy equ^{n} (9) at each TIR bounce. Thus at each bounce point we have two SHs generated having a certain spatial separation among themselves which in turn depends on the optical dispersion and the angle of incidence. The spatial separation thus evolved has a cumulative effect and goes on increasing with the progression of the waves throughout the slab length resulting in two adverse effects: firstly a spatial walk off between the interacting waves thereby reducing the overlapping between the beams. Secondly the pump and parametric beams may recombine after a certain number of bounces given by $N_{rec} \approx 2\left|tan\phi_{\omega}/\delta\phi\right| \approx 2\left|\frac{n}{\delta n}\right|$ [20], depending on the slab length; after which the generated beam will fill the plate completely. This recombination may cause a destructive interference effect which will reduce the efficiency further.

For a particular frequency inside the fundamental broadband source, the value of *(δn/n)* will remain constant but if the angle of incidence Φ_{ω}, which depends on the geometry of the slab, varies at each bounce, then the angular difference between the collinear SH and the homogeneous SH will also vary with the propagation of the beam throughout the slab length. Now the double tapered configuration used in Ref. [7] combines a forward and a reverse tapered section. Since the angle of incidence inside the slab being dependent on tapering angles, will first increase and then decrease, the beam separation will also accordingly increase and then decrease.

Now when we have considered the effect of this nonlinear reflection in our proposed slab configurations, in config. 1, the angle of incidence Φ_{ω} inside the slab will go on increasing depending on the value of $(\theta_1 + \theta_2)$ which will increase the spatial separation among the interacting waves inside the slab resulting in more pronounced effect as compared to parallel slab. In case of config. 2, the angle of incidence inside the slab will also go on increasing but the magnitude of increase in subsequent TIR point will be less as compared to config. 1 because here the angle of incidence depends on the value of $(\theta_1 - \theta_2)$. Now in config. 3, the angle of incidence inside the slab will first go on decreasing in the first tapered section and then it will increase in the second tapered section. Thus the beam separation will also vary accordingly.

Now let us try to extend our analysis in the following manner: At each TIR bounce point, due to the generation of two SHs namely collinear and homogeneous, we have two fields generated. The collinear SH generated at the first TIR bounce point is calculated considering the dispersion phase shift corresponding to the first bounce length from the entry point in a manner similar to that already explained in Ref. [7]. Then at the same bounce point we have determined the radiated homogeneous SH field which is travelling with an angular shift of $\delta\Phi$ with respect to the collinear SH. The net SH field amplitude has been calculated at this bounce point considering the relative phase shift between the two waves. Now at the consecutive bounce points we have similarly calculated the SH field due to the collinear and homogeneous SHs generated at that point considering Fresnel phase shift along with the dispersion phase shift (ΔkL_n) and angular phase shift due to nonlinear reflection. However, in *ppp* polarization configuration, d coefficient does not undergo a sign change on TIR bounce; therefore, the additional phase shift has not been considered. The SH field of the previous bounce point will also contribute to the newly generated SH at the next bounce point but with a relative Fresnel phase shift and dispersion phase shift. Thus the total SH field at each bounce point has to be calculated considering the contribution of the previous SH along with its phase shift term. The wave vector, also being dependent on the cosine of $\delta\Phi_n$ (= $(k_1 - k_2)\cos\delta\Phi_n - k_1$), needs to be calculated for each step [20]. Finally the net electric field contribution due to collinear as well as homogenous SHs generated inside the double tapered slab during propagation of the optical beam throughout the slab length will be obtained. The effect of spatial walk-off which decreases the overlap between the interacting beams has been calculated using the expression used for the birefringence walk-off correction term developed by Smith *et. al.* [21] given as $\frac{1}{\sqrt{1+0.51(\rho L/W)^2}}$, where, $\rho = \frac{1}{n}\frac{\delta n}{\delta\theta}$ is the walk-off angle, L is the interaction length and W is the Gaussian beam width.

4. Results and discussions

A computer aided simulation has been carried out for the proposed semiconductor slabs using MATLAB software for *ppp* polarization configuration. In the present analysis a beam waist of 100 μm has been considered which gives Rayleigh length ranging between 0.9 - 1.6 cm corresponding to a centre wavelength of the fundamental broadband radiations. The optical path length has been calculated by summing up all the bounce lengths inside

each of the slab. Based on this we have considered a slab length of 7 mm so that the total interaction path length inside the slab remain less than or equal to its corresponding Rayleigh length. The thermal expansion coefficients for GaAs, ZnSe and ZnTe materials are 5.8 x 10^{-6}/K [5], 7.8 × 10^{-6}/K [5] and 8.19× 10^{-6}/K [22]respectively. The analysis uses an input fundamental broadband source of (7-7.9) μm,(4.6-5.8) μm and (6.8-8.1) μm for GaAs, ZnSe and ZnTe respectively. The operating temperature of 298 K for GaAs and ZnSe made configurations and 293 K for ZnTe made configurations are used in our computer aided simulation.

Now in the subsequent paragraphs the configuration wise performance analysis of all the three slabs have been presented.

4.1. Analysis of performance parameters of Config. 1

With reference to Fig. 1(a), we have choosen t_1= 400 μm, t_2= 2 μm, t_3= 3 μm, and L= 7 mm. Fig. 6 shows the graphical representation of fundamental wavelength vs. SH conversion efficiency under ideal as well as lossy condition including the effect of nonlinear law of reflection for GaAs, ZnSe and ZnTematerials.

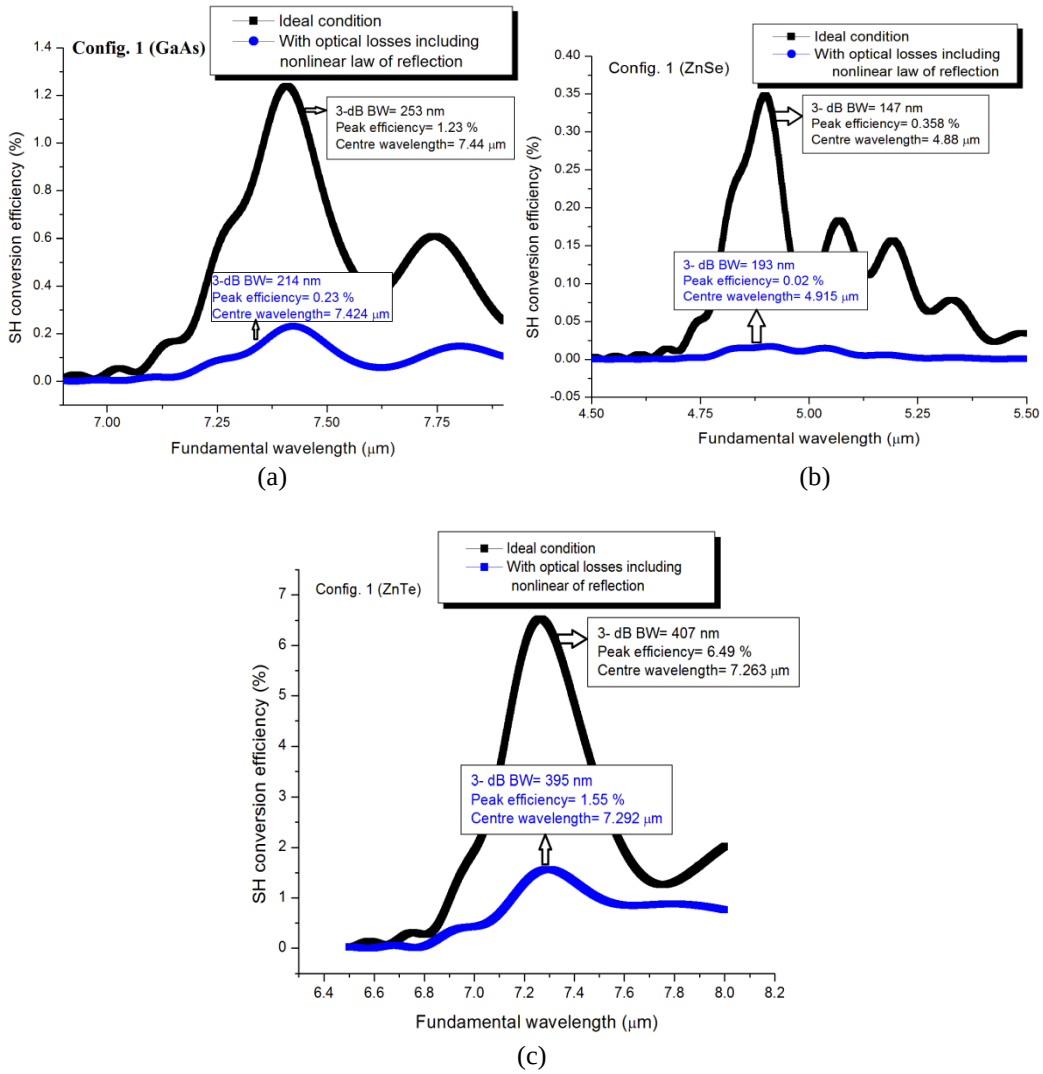

Fig. 6. Variation of SH conversion efficiency w.r.t. fundamental wavelength for config. 1 (a) GaAs (b) ZnSe and (c) ZnTe

4.2. Analysis of performance parameters of Config. 2

With reference to Fig. 1(b), the slab parameters t_1, t_2, t_3 and L are considered as same as config. 1. The graphical representation of fundamental wavelength vs. SH conversion efficiency under ideal as well as lossy condition including the effect of nonlinear law of reflection are shown in Fig. 7 for GaAs, ZnSe and ZnTe materials.

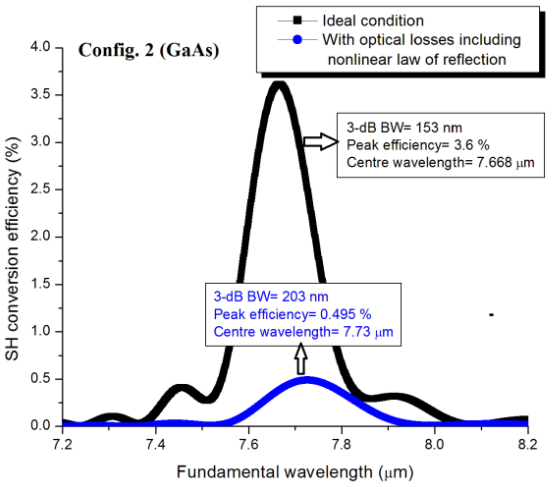

(a)

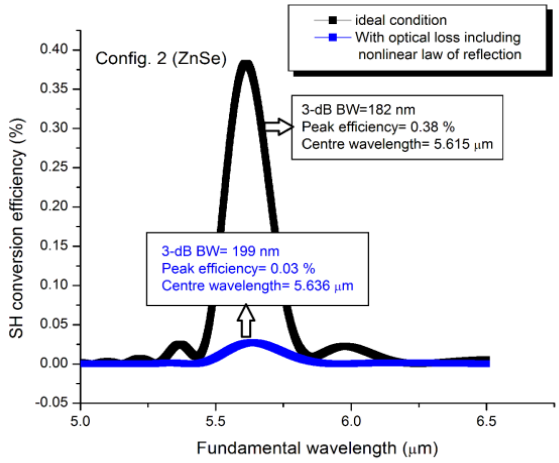

(b)

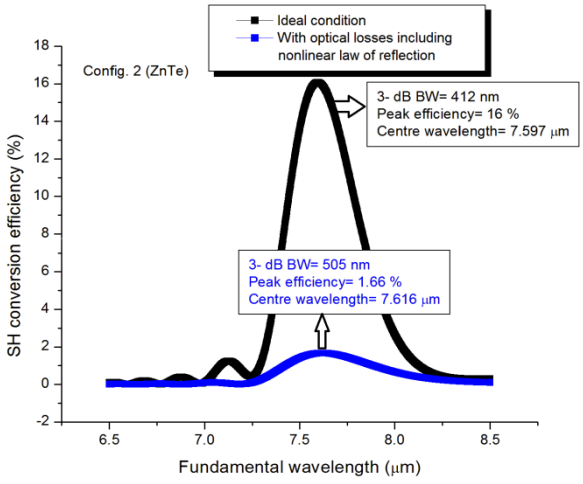

(c)

Fig. 7. Variation of SH conversion efficiency with respect to the fundamental wavelength for config. 2 (a) GaAs (b) ZnSe and (c) ZnTe

4.3. Analysis of performance parameters of Config. 3

For configuration 3, with reference to Fig. 1(c), we have choosen t_1=400 μm, t_2= 395 μm, L= L_R + L_F = 7 mm (L_R= 2 mm and L_F= 5 mm). Fig. 8 shows the variation of SH conversion efficiency with respect to the fundamental wavelength under ideal as well as lossy condition including the effect of nonlinear law of reflection for GaAs, ZnSe and ZnTe materials.

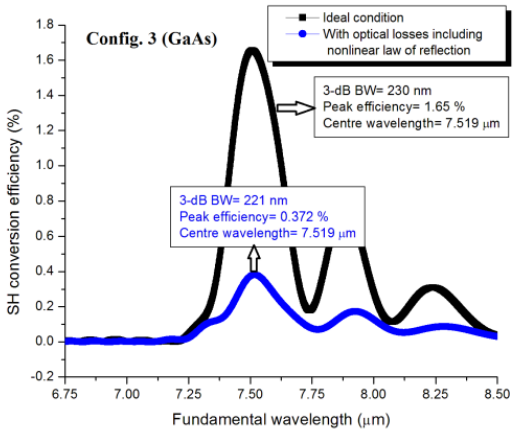

(a)

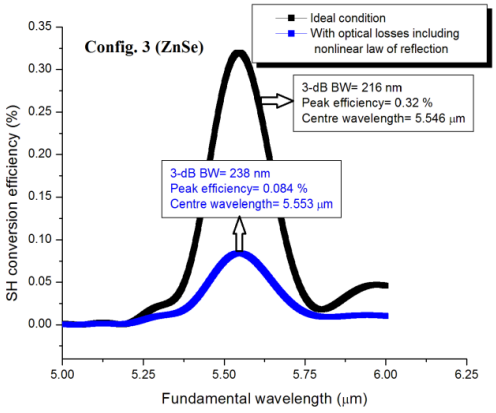

(b)

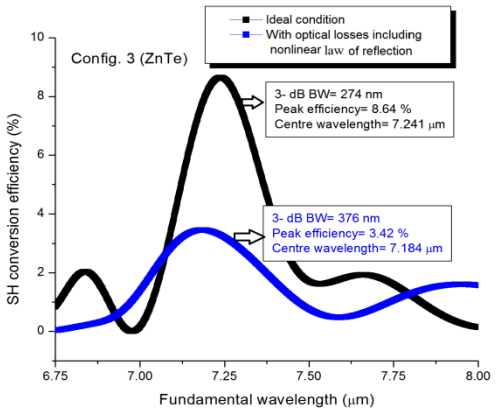

(c)

Fig. 8. Variation of SH conversion efficiency with respect to the fundamental wavelength for config. 3 (a) GaAs (b) ZnSe and (c) ZnTe

4.4. Analysis of performance parameters of Config. 4

In config. 4 we have simulated the double tapered slab structure as analyzed in ref. [7] with dimensions comparable with that of our presently proposed three configurations discussed above. Here we have choosent$_1$= 400 μm, t$_2$= 405 μm and L= 7 mm. Fig. 9 shows the variation of SH conversion efficiency with respect to the fundamental wavelength under ideal as well as lossy condition including the effect of nonlinear law of reflection for GaAs, ZnSe and ZnTe materials.

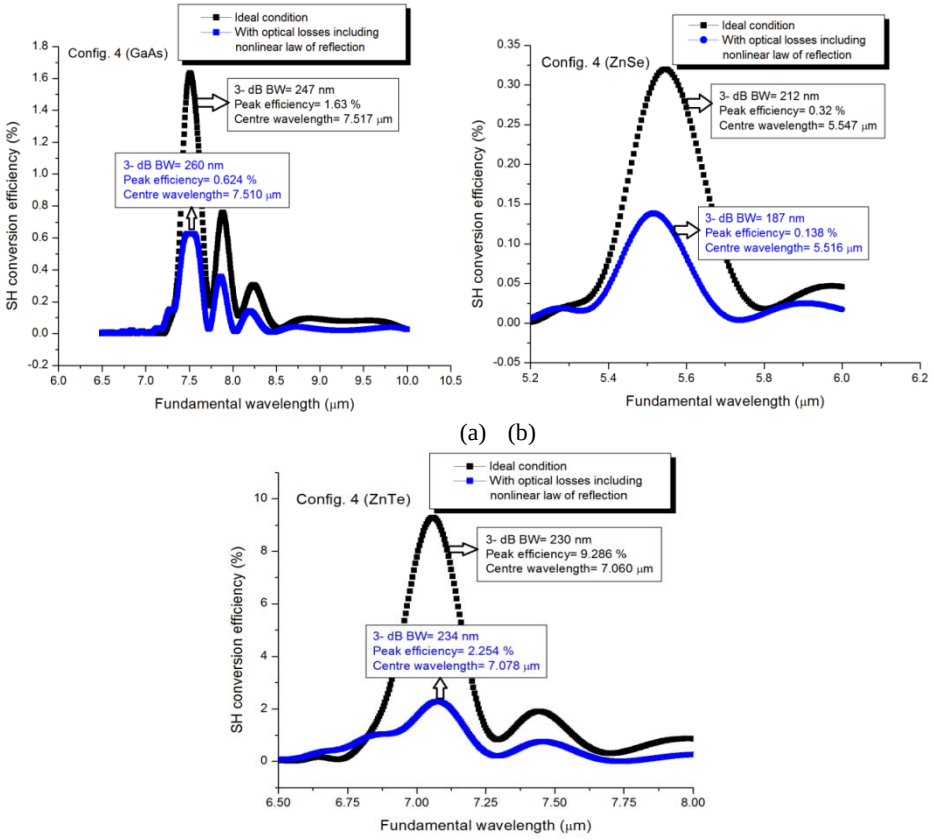

Fig. 9. Variation of SH conversion efficiency with respect to the fundamental wavelength for config. 4 (a) GaAs (b) ZnSe and (c) ZnTe

Table 2. Comparative analysis of the proposed broadband frequency converters with the original double tapered configuration [7]

Config.	Material	Incident angle (rad)	Ψ (rad)	Peak conversion efficiency (%)		Centre wavelength of fundamental (μm)		3- dB BW (nm)	
				Ideal	With optical loss including nonlinear law of reflection	Ideal	With optical loss including nonlinear law of reflection	Ideal	With optical loss including nonlinear law of reflection
Config. 1	GaAs	1.4	0.7	1.23	0.23	7.44	7.424	253	214
	ZnSe	1.4	0.5	0.358	0.02	4.88	4.915	147	193
	ZnTe	1.4	0.7	6.49	1.55	7.263	7.293	407	395
Config. 2	GaAs	1.4	0.6	3.6	0.495	7.668	7.73	153	203
	ZnSe	1.4	0.3	0.38	0.03	5.615	5.636	182	199
	ZnTe	1.4	0.55	16	1.66	7.597	7.616	412	505
Config. 3	GaAs	1.4	0.6	1.65	0.372	7.519	7.519	230	221
	ZnSe	1.4	0.3	0.32	0.084	5.546	5.553	216	238
	ZnTe	1.4	0.4	8.64	3.42	7.241	7.184	274	376
Config. 4 [7]	GaAs	1.4	0.7	1.63	0.626	7.517	7.546	247	267
	ZnSe	1.4	0.3	0.32	0.138	5.547	5.516	212	187
	ZnTe	1.4	0.65	9.286	2.254	7.060	7.078	230	234

Table 2 tabulates the comparative analysis in the four different configurations.

5. Conclusions

In this paper, a comparative study in terms of peak conversion efficiency and 3- dB BW have been analyzed numerically on four different double tapered configurations made of either GaAs or ZnSe or ZnTe semiconductor material using TIR QPM based SHG technique considering ideal case as well as lossy condition including destructive interference effect due to the nonlinear law of reflection. When the catastrophic effect due to nonlinear law of reflection has been incorporated, heavy drop has been observed in the peak efficiency with GaAs, ZnSe and ZnTe materials in all the configurations. The computed efficiency and the 3 dB BW seem to be much superior for ZnTe compound as compared to either GaAs or ZnSe compound. Config. 3 seems to be the favourable choice in terms of conversion efficiency whereas config. 2 provides the best result when BW is the prime concern. Thus with proper choice of the related operating conditions, one can design a highly efficient broadband frequency converter of desired BW in various regions particularly of the mid IR spectra using different isotropic semiconductors finding useful applications in spectroscopy, remote sensing, and IR countermeasures [23]. The proposed broadband converter may also come forward in the same line with quantum cascade (QC) lasers which constitute a type of semiconductor lasers capable of emitting light in the mid and far IR spectral regions. The proposed broadband converter also allows fine tuning of the fundamental centre wavelength of the output 3 dB BW by varying the operating temperature in case of GaAs and ZnSe as shown in Table 3. For simulating the effect of temperature variation in GaAs and ZnSe we have choosen config. 4 where the SH conversion efficiency and BW product is the highest among the four configurations.

Table 3. Temperature tuning for GaAs and ZnSe materials

Material	Operating Temperature (K)	Centre wavelength of fundamental (μm)	Peak efficiency (%)	3- dB BW (nm)
GaAs	298	7.546	0.626	267
	308	7.571	0.625	267
	318	7.592	0.622	267
	328	7.613	0.622	275
ZnSe	298	5.516	0.138	187
	308	5.523	0.138	188
	318	5.530	0.138	188
	328	5.541	0.138	188

In case of GaAs when temperature has been varied from 298 K to 328 K in steps of 10 K, the centre wavelength corresponding to peak efficiency shows a red shift of 67 nm with very nominal variation in efficiency and bandwidth. The relative drop in efficiency is only 0.6 % while the BW rises by only 8 nm. In ZnSe for similar variation in temperature, a red shift of 25 nm is obtained in the centre wavelength where the efficiency remains constant with a corresponding change in BW by 1 nm. These observations lead to the conclusion that temperature tuning results in a finer control of centre wavelength in ZnSe as compared to GaAs. The variations in conversion efficiency as well as 3-dB BW are also comparatively less prominent in case of ZnSe.

References

[1] J. A. Armstrong, N. Bloembergen, J. Ducuing, P. S. Pershan, Phys. Rev. **127**, 1918 (1962).
[2] G. D. Boyd, C. K. N. Patel, Appl. Phys. Lett. **8,** 313 (1966).
[3] H. Komine, W. H. Long, Jr., J. W. Tully, E. A. Stappaerts, Opt. Lett. **23,** 661 (1998).
[4] R. Haïdar, N. Forget, Ph. Kupecek, E. Rosencher, J. Opt. Soc. Am. B **21**, 1522 (2004).
[5] A. Saha, S. Deb, Opt. Comm. **284**, 4714 (2011).
[6] S. Deb, A. Saha, Optik, **124**, 2428 (2013).
[7] A. Saha, S. Deb, Optik – International Journal for Light and Electron Optics**125**, 6861 (2014).
[8] M. Raybaut, A. Godard, A. Toulouse, C. Lubin, E. Rosencher, Opt. Exp. **16**, 18457 (2008).
[9] T. Skauli, P.S. Kuo, K.L. Vodopynaov, T. J. Pinguet, O. Levi, L. A. Eyres, J. S. Harris, M. M. Fejer, B. Gerard, L. Becouarn, E. Lallier, Journal of Appl. Phys. **94**, 6447 (2003).
[10] T. Skauli, K.L. Vodopynaov, T. J. Pinguet, A. Schober, O. Levi, L. A. Eyres, M. M. Fejer, J. S. Harris, B. Gerard, L. Becouarn, E. Lallier, G. Arisholm, Opt. Lett. **27**, 628 (2002).
[11] A. Mustelier, E. Rosencher, Ph. Kupecek, A. Godard, M. Baudrier, M. Lefebvre, M. Poulat, G. Mennerat, C. Pasquer, P. Lemasson, Appl. Phys. Lett. **84**(22), 4424 (2004).
[12] R. L. Sutherland, Handbook of Nonlinear Optics (Marcel Dekker, Second Ed., New York, 1975).
[13] http://www.almazoptics.com/GaAs.htm, May 2014.
[14] BabakImangholi, Michael P. Hasselbeck, Mansoor Sheik- Bahae, Opt. Comm. **227**, 337 (2003).
[15] http://www.ClevelandCrystals.Inc.II-VI Crystals.htm, May 2013.
[16] R. Haidar, P. Kupecek, E. Rosencher, Appl. Phys. Lett. **83**, 1506 (2003).
[17] R. Haidar, Ph. Kupecek, E. Rosencher, R. Triboulet, Ph. Lemasson, Opto- electronics Reviews **11**, 155 (2003).
[18] N. Lovergine, D. Manno, A. M. Mancini, L. Vasanelli, J. Cryst. Growth, **128**, 633 (1993).
[19] H. H. Li, J. Phys. Chem. Ref. Data **13**, 103 (1984).

[20] N. Bloembergen, P.S. Pershan, Phys. Rev. **128**, 606 (1962).
[21] A. V. Smith, D. J. Armstrong, W. J. Alford, J. Opt. Soc. Am. B **15**, 122(1998).
[22] L. I. Berger, Semiconductor materials, (CRC Press, 1997).
[23] O. Levi, T. J. Pinguet, T. Skauli, L. A. Eyres, K. R. Parameswaran, J. S. Harris, Jr., M. M. Fejer, T. J. Kulp, S. E. Bisson, B. Gerard, E. Lallier, L. Becouarn, Opt. Lett. **27**, 2091 (2002).

*Corresponding author: sumita_nita@rediffmail.com